Catena 173 (2019) 234–245

Contents lists available at ScienceDirect

Catena

journal homepage: www.elsevier.com/locate/catena

Runoff-sediment dynamics under different flood patterns in a Loess Plateau catchment, China

Jinfei Hu[b,c], Peng Gao[a,b,*], Xingmin Mu[a,b], Guangju Zhao[a,b], Wenyi Sun[a,b], Pengfei Li[b], Limei Zhang[a]

[a] State Key Laboratory of Soil Erosion and Dryland Farming on the Loess Plateau, Northwest A&F University, Xinong Road 26, Yangling 712100, Shaanxi Province, China
[b] Institute of Soil and Water Conservation, Chinese Academy of Sciences & Ministry of Water Resources, Xinong Road 26, Yangling 712100, Shaanxi Province, China
[c] University of Chinese Academy of Sciences, Beijing 100049, China

ARTICLE INFO

Keywords:
Event scale
Runoff–sediment relationship
Flood patterns
Hysteresis loop
Sediment dynamics

ABSTRACT

Investigating the suspended sediment dynamic is useful for gaining a more comprehensive understanding of runoff and sediment yield process. The study analyzes the sediment flow behavior in relation to the flood patterns in the Xichuan River catchment on the Loess Plateau. Based on 23-year hydrological data collected from Zaoyuan hydrological station and K-medoids clustering method, one hundred and twelve flood events data were classified into four flood patterns. The hydrologic features of different flood patterns exhibit significant differences. The values of the mean runoff depth, the mean flood duration, and the mean flood peak discharge decreased as the following order: Pattern A > Pattern C > Pattern D > Pattern B. Each flood pattern results in differing levels of the event sediment yield (SY), the SY of Pattern A (10,275.33 $t \cdot km^{-2}$) and Pattern C (1196.39 $t \cdot km^{-2}$) were larger than those from Pattern B (218.84 $t \cdot km^{-2}$) and Pattern D (693.84 $t \cdot km^{-2}$). These results indicated that greater attention should be paid to Pattern A and Pattern C because of the largest sediment delivery effect. Multiple stepwise regressions analysis suggested that the contribution of main runoff-related factors to event sediment yield varied with different flood patterns. In addition, hysteretic analysis between suspended sediment concentration and runoff suggested that counter-clockwise and figure-eight loops were the dominant loops. The results provided a useful information to flood pattern classifications and suspended sediment dynamics research, and enriched the sediment control theory at the watershed scale.

1. Introduction

Suspended sediment transport, which is a complex process related to rainfall characteristics, runoff discharge and sediment availability, is significantly influenced by spatial-temporal heterogeneity of hydrological and geomorphological process (Zabaleta et al., 2007). Rainfall plays a critical role in soil-particle detachment, whereas the surface runoff is the fundamental driving force for sediment delivery, which is a necessary prerequisite for sediment-laden flow transportation processes during individual hydrological events. Accordingly, a growing need for studying suspended sediment dynamics has been noticed by numerous researchers due to its significant ecological and environmental effects (Fang et al., 2011; Oeurng et al., 2010; Sun et al., 2016). It will be beneficial for the improvement of our understanding on the spatial distribution and dynamic of sediment through exploring the relationship among rainfall, runoff and sediment (Asselman, 1999; Porto et al., 2011; Zhao et al., 2016).

The suspended sediment concentration and discharge (SSC-Q) hysteresis types could be employed to interpret suspended sediment dynamics. The shapes of hysteretic loops, including clockwise, counter-clockwise, figure-eight and complex, are useful to determine the sediment availability and the approximate spatial distribution of sediment sources of a single event within the drainage system (Buendia et al., 2016; Lefrançois et al., 2007). For example, Fang et al. (2011) investigated various patterns of SSC-Q hysteresis loops at different temporal scales, indicating that the sediment dynamic change of storage seasons could be explained by the seasonal 'store-release' process. Using the SSC-Q relationship, Zhao et al. (2017) explored the potential causes of variations in runoff and sediment load from three driving forces: climate changes, soil and water conservation measures and check dams, and pointed out the effect of human activities on the runoff-sediment dynamics. Despite a number of researches on sediment dynamics and

* Corresponding author at: State Key Laboratory of Soil Erosion and Dryland Farming on the Loess Plateau, Northwest A&F University, Xinong Road 26, Yangling 712100, Shaanxi Province, China.
E-mail address: gaopeng@ms.iswc.ac.cn (P. Gao).

https://doi.org/10.1016/j.catena.2018.10.023
Received 28 October 2017; Received in revised form 13 October 2018; Accepted 18 October 2018

hysteretic relationships at different spatial and temporal scales (Bača, 2008; Deasy et al., 2009; López-Tarazón et al., 2009; Sayer et al., 2006), relatively limited studies have been conducted to understand the sediment transport processes under various hydrologic patterns. In addition, the restriction of field monitoring and data collection prevents further investigations of the event-based sediment dynamics within the large-scale and meso-scale systems (Tian et al., 2016). It was thus essential to fully investigate the hydro-sedimentary dynamic of meso-scale watershed, and the runoff–sediment relationship under various flood patterns.

The Loess Plateau, located in the upper and middle reaches of the Yellow River in northwestern China, has been suffered from severe soil erosion, which harms local ecosystem and social economy seriously (Mu et al., 2007; Tang et al., 1991; Zhao et al., 2013). During the past several decades, a series of soil and water conservation measures and eco-rehabilitation strategies have been implemented to greatly reduce the soil erosion rates and decreased the sediment load of Yellow River (Wang et al., 2007). The main objectives were to (i) examine the dominant hydrological variables that have a major influence on sediment yield and delivery by analyzing the relationship between rainfall, discharge and sediment at the flood event scale, (ii) explore the relationship between the sediment yield and predominated hydrologic variables under different patterns of flood events, (iii) identify the sediment sources of different SSC-Q hysteresis loops.

2. Material and methods

2.1. Study area

The Yanhe catchment covers an area of 7725 km^2 in the south of the Loess Plateau. This basin is characterized by steep gullies, suffering from severe soil erosion and extremely high sediment yields (Wang et al., 2015). It has a typical temperate continental semi-arid monsoon climate with an average annual rainfall of 500–550 mm. The main surface material of the basin is fine loess soil.

The Xichuan River catchment is one of the first-order tributaries of the Yanhe River (Fig. 1). The catchment covers an area of approximately 801 km^2, with altitude varying from 800 m to 1600 m and the main river length of 65.3 km. The drainage area gauged by Zaoyuan station (N 36°38′; E 109°20′) is 719 km^2, about 13 km apart from the estuary. The average annual temperature is 9.4 °C and the average annual precipitation is 520.0 mm. The annual precipitation exhibits an extremely uneven characteristic and most of the precipitation in this area falls between May and September in the form of short-duration, high-intensity rainstorms. Consequently, runoff is mostly concentrated in the rainy season (Bai, 2011). In addition, rainstorms lead to severe soil erosion and extraordinarily high sediment yields. The average annual runoff and sediment load at the hydrological gauging station are 2.17×10^7 m^3 (31 mm/a) and 3.15×10^6 t (4,437 t/km^2/a), respectively, between 1971 and 2013.

2.2. Data sources

Since the 1950s, the Yellow River Commission Committee has set up numerous hydrologic stations to monitor flow and sediment process to reflect erosion and sediment yield in the Loess Plateau. The precipitation data acquired from six rainfall gauge stations distributed across the study area. Runoff and sediment data since 1974 were collected at the Zaoyuan hydrologic station, which was situated within the Xichuan river watershed in Yan'an City, Shaanxi Province. Rainfall, runoff and suspended sediment transport data at these gauge stations were acquired from the Yellow River Hydrological Year book (Yellow River Conservancy Committee, 1974), which was issued by Yellow River Conservancy Commission (YRCC) of the Ministry of Water Resources of People's Republic of China (PRC).

Water levels, sediment concentrations and precipitation were continuously monitored to explore precipitation conditions, hydrological responses and sediment dynamics. For the majority of the flood events, the duration of flood process lasted for merely a short period of time. Therefore, to capture the hydrological processes during floods, the sampling interval was intensive (6 or 12 min) during the peak flow period, but after floods, it was generally 4–6 h. The water level was measured by an automatic water level recorder, then the water level could be transformed into runoff by means of the calibrated runoff–-water level curves. Sediment flow sampling was undertaken using horizontal samplers or bottles. The suspended sediment concentration was obtained by the gravimetric method in a laboratory. The sample concentrations were determined using a displacement formula in cases of high concentrations. For a more detailed information about this method, kindly refer to Zheng et al. (2015). At low sediment concentration, the runoff samples with sediment were settled separated from the water through a filter, and then the residue was oven dried at 105 °C for 24 h. The weight of each dried residue and the sample volume provided the SSC. The sample concentration then could be used as a surrogate for the cross-section concentration. The sediment yield could then be calculated based on runoff, suspended sediment concentration, and time interval for a single flood event. The whole process, including hydrological survey, sampling and experimental determination, followed international standards and methods entirely, and all the data have been verified strictly when they were published.

Rainfall, runoff and suspended sediment transport data at these gauge stations were acquired from the Yellow River Hydrological Year book (Yellow River Conservancy Committee, 1974), which was issued by Yellow River Conservancy Commission (YRCC) of the Ministry of Water Resources of People's Republic of China (PRC). Single complete flood event can be conceptually considered as: starting when stream increase above the base flow to the time when merely base flow contribute to discharge (Eder et al., 2010). The impact of base flow on the total runoff during the flood events was fairly limited, hence, base flow separation was not processed in this study. In order to exclude flood events with low sediment transport rate in the channel, some reasonable restrictions were essential to set: runoff depth is in excess of 0.10 mm, flood peak discharge is higher than 7.50 $m^3 \cdot s^{-1}$ and the flood duration is longer than 250 min. According to the presupposed standard above, a total of 112 flood events and the corresponding rainfall process which occurred between 1974 and 2013 (data during the period 1990–2006 were missing) were selected for the analysis of the runoff-sediment relationships.

Land use data at a spatial resolution of 30 m for 1990 and 2010 were provided by the Data-Sharing Network of China Earth System Science (www.geodata.cn). Based on high resolution Landsat TM images, the land use databases were developed by visual interpretation and digitalization. The data quality and results were verified by field campaigns before their release. The land use of Xichuan River basin is classified into six types: forest, grassland, bare or unused land, arable land, water body and urban area.

2.3. Methods for data analysis

For each flood event, the various hydrological variables were used to describe the individual flood hydrographs and sediment delivery characters, and the related variables of runoff, sediment, and precipitation are listed in Table 1.

For a specific flood event, the time interval for the hydrological observations is assumed as Δt, instantaneous discharge and suspended sediment concentration is Q_t and S_t, respectively, and the controlled area of the Zaoyuan hydrologic station is A. The flood runoff depth (H) is calculated as follows:

$$H(t_1, t_2) = \frac{\int_{t_1}^{t_2} Q_t \, d_t}{A} = \frac{\sum Q_t \Delta t}{A} \quad (1)$$

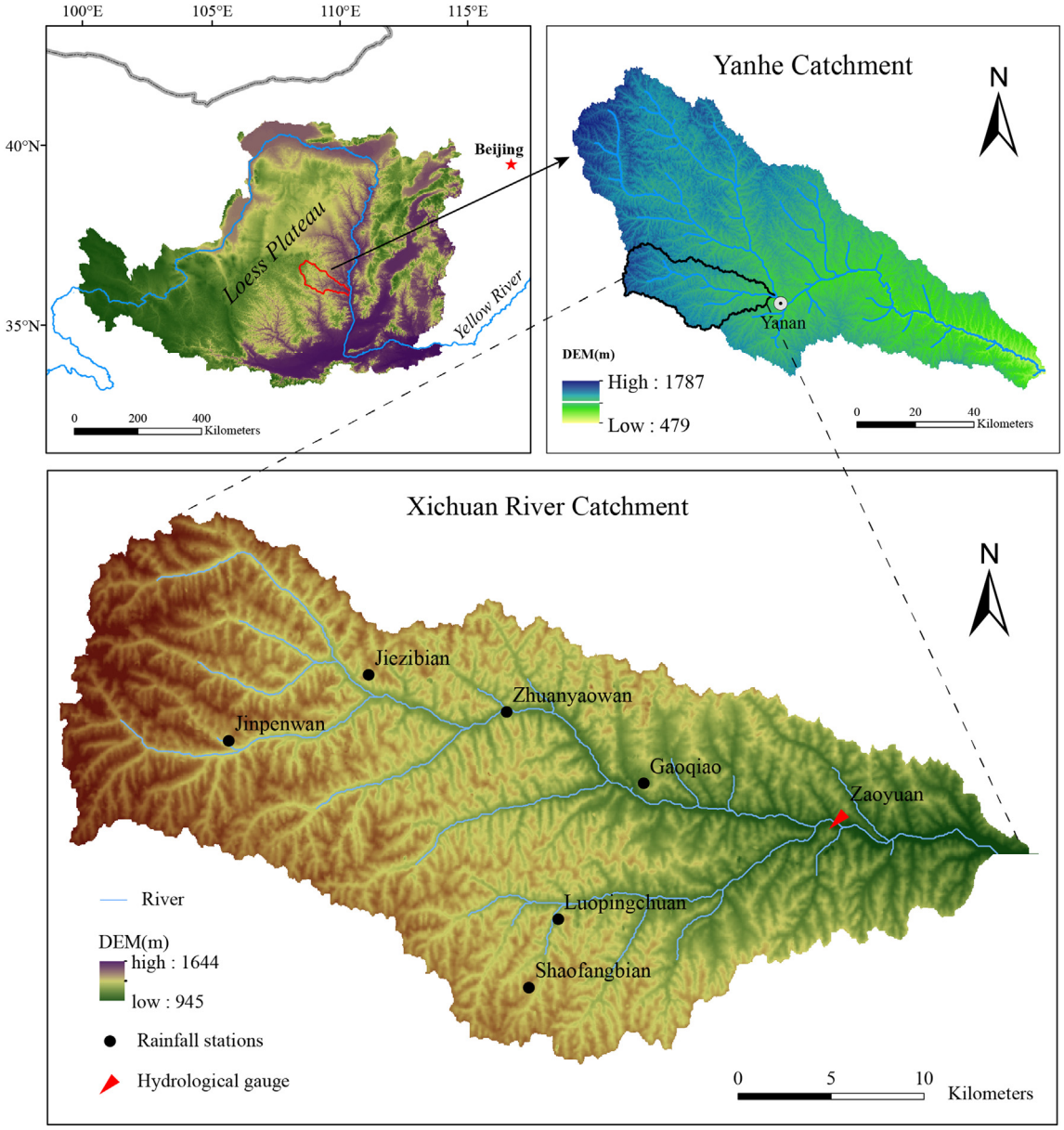

Fig. 1. Location of the Xichuan River catchment.

Table 1
Flood variables and corresponding abbreviations.

Runoff-relevant variable	Sediment-relevant variable	Precipitation-relevant variable
Flood runoff depth (H, mm)	Event sediment yield (SY, $t{\cdot}km^{-2}$)	Total precipitation (P, mm)
Flood duration (T, min)	Mean suspended sediment concentration (SSC, $kg{\cdot}m^{-3}$)	Rainfall intensity (I, $mm{\cdot}h^{-1}$)
Peak discharge (Q_p, $m^3{\cdot}s^{-1}$)	Maximum suspended sediment concentration (S_{max}, $kg{\cdot}m^{-3}$)	
Mean discharge (Q_m, $m^3{\cdot}s^{-1}$)		
Flow variability (*FV*)		

The sediment yield (SY) for a flood event within the interval (t_1, t_2) can be calculated as:

$$SY(t_1, t_2) = \frac{\int_{t_1}^{t_2} S_t Q_t dt}{A} = \frac{\sum S_t Q_t \Delta t}{A} \quad (2)$$

The flow variability is defined as the ratio of flood peak discharge (Q_p) to mean discharge (Q_m), then the following formula can be obtained:

$$FV = \frac{Q_p}{Q_m} \quad (3)$$

By using the hydrological variables above, we investigated the flood events for the periods from 1974 to 1989 and 2007 to 2013 to better understand the runoff-sediment dynamics under different flood patterns.

Clustering analysis has been widely adopted to categorize objects in accordance with their resemblance in scientific fields (Peng and Wang, 2012). Among the numerous clustering methods, K-medoids uses squared Euclidean distance measure and the k-means + + algorithm for choosing initial cluster medoid positions, and the group number is required to determine before classification. Discriminant analysis was applied to determine the optimal clusters by Fisher's discriminant function. In the current study, 112 flood events were selected as the statistical sample, K-medoids and discriminant analysis were applied to

classify the flood events according to T, H, and Q_p. The classifications of flood events met the ANOVA criterion at the 0.001 significant level. The Fisher's discriminant functions that were employed in the discriminant analysis were showed as follows:

$$G_1 = 1.049H + 0.087T + 0.069Q_p - 166.187 \quad (4)$$

$$G_2 = -0.453H + 0.025T + 0.01Q_p - 9.455 \quad (5)$$

$$G_3 = -0.461H + 0.064T + 0.022Q_p - 55.735 \quad (6)$$

$$G_4 = -0.523H + 0.043T + 0.017Q_p - 25.765 \quad (7)$$

where G_k (k = 1, 2, 3, 4) is the classification score for group k.

The discharge and suspended sediment concentration values of flood events were used to draw and analyze SSC-Q hysteresis loops. In general, the hysteresis loops mainly include four shapes, namely clockwise, counter-clockwise, figure-eight, and complex loop (Tian et al., 2016; Williams, 1989), which could be employed to reflect the variations in sediment sources and sediment depletion (Buendia et al., 2016). The hysteresis loops reflect the SSC-Q behavior, and was also related to suspended sediment dynamics in the sediment supply and sediment transport process at the event scale (Luk, 1997; Soler et al., 2008).

3. Results

3.1. Sediment yield variations among flood events

Table 2 shows the frequency distribution of flood event sediment yield in the Xichuan River basin during 1974–1989 and 2007–2013. All the flood events were divided into five levels according to the magnitude of sediment yield: relative small flood events (0–100 $t{\cdot}km^{-2}$), small flood events (100–1000 $t{\cdot}km^{-2}$), medium flood events (1000–5000 $t{\cdot}km^{-2}$), large flood events (5000–10,000 $t{\cdot}km^{-2}$) and extremely large events (> 10,000 $t{\cdot}km^{-2}$).

Among the 112 flood events, there was only one extremely large flood event with sediment yield > 10,000 $t{\cdot}km^{-2}$. The occurrence frequency of small flood events was much more often than any other level events, reached up to 52%. There were 36 extreme small flood events and 16 medium flood events, accounting for 32% and 14% of the total, respectively.

Table 3 shows the different characteristics of rainfall, runoff and suspended sediment for the 112 flood events in the Xichuan River catchment. According to descriptive statistics of selected flood events, almost all variables fluctuated in a wide scope in the period 1974–1989 and 2007–2013. The duration of the flood events ranged from 252 to 2160 min, with an average value of 1008.2 min. The proportion of flood events that exceed 1500 min account for about 8.9%, merely 10 events, however, up to 50% of the flood events whose duration was shorter than the average value. H varied from 0.12 mm to 22.04 mm, with a mean value of 1.90 mm. There were 81 flood events with H lower than 1.90 mm, and 8 events having that > 5 mm. The average of Q_p was 165.50 $m^3{\cdot}s^{-1}$, and the highest value reached 2460 $m^3{\cdot}s^{-1}$, with the minimum of 7.94 $m^3{\cdot}s^{-1}$. *FV* ranged from 1.88 to 53.79, with an average value of 6.64, the magnitude of *FV* was generally small: merely 17 events (15.2%) exceeded 10, by contrast, 61.6% of the total events were lower than 6.

Table 2
The frequency distribution of flood event sediment yield.

Station	Sediment yield ($t{\cdot}km^{-2}$)					Total
	0–100	100–1000	1000–5000	5000–10,000	> 10,000	
Zaoyuan	36	58	16	1	1	112
	Frequency of occurrence (%)					
	32%	52%	14%	1%	1%	100%

Table 3
Descriptive statistics of rainfall-runoff-sediment events.

Variables	Statistical description				
	Max.	Min.	Mean	Std. dv.	CV
T/min	2160.00	252.00	1008.16	397.23	0.39
H/mm	22.04	0.12	1.90	3.08	1.62
$Q_p/m^3{\cdot}s^{-1}$	2460.00	7.94	165.50	310.76	1.88
$Q_m/m^3{\cdot}s^{-1}$	115.88	1.56	17.54	20.98	1.2
FV	53.79	1.88	6.64	5.88	0.88
P/mm	101.10	1.65	23.06	19.70	0.85
$I/mm{\cdot}h^{-1}$	45.88	0.60	5.47	6.33	1.16
$SY/t{\cdot}km^{-2}$	11,033.40	12.69	749.88	1561.34	2.08
$SSC/kg{\cdot}m^{-3}$	901.36	33.92	314.31	155.67	0.50
$S_{max}/kg{\cdot}m^{-3}$	975.00	41.10	482.29	192.11	0.40

The SY of flood events had a range of 12.69–11,033.40 $t{\cdot}km^{-2}$, with a mean value of 749.88 $t{\cdot}km^{-2}$. Flood events with SY larger than 3000 $t{\cdot}km^{-2}$ were merely observed in extremely low frequency (7 events), nevertheless, events below 800 $t{\cdot}km^{-2}$ occupied a large portion of the total events, which could reach up to 91 times (81.2%). SSC varied from 33.92 $kg{\cdot}m^{-3}$ to 901.36 $kg{\cdot}m^{-3}$ with an average of 314.31 $kg{\cdot}m^{-3}$. S_{max} had a range between 41.102 $kg{\cdot}m^{-3}$ and 975.00 $kg{\cdot}m^{-3}$, and the events with S_{max} > 500 $kg{\cdot}m^{-3}$ accounted for approximately 54.5% of the total events. Additionally, the coefficient of variation (CV) of SSC and S_{max} was relatively low compared with the Q_p and Q_m.

3.2. Correlation among rainfall, runoff, and sediment yield

Fig. 2 shows the simple regression among different variables of flood events. A wide range of sediment responses to flood runoff were found in the study area. The SY had extremely remarkable correlations ($p < 0.01$) with hydrological variables (H, Q_p, Q_m, and *FV*). In particular, the strongest linear correlation was detected between H and SY with a correlation coefficient of 0.98. Thus, H was the most primary variable influencing the event sediment yield of the basin. On the other hand, SSC and S_{max} were well correlated with hydrological variables, suggesting that total runoff volume, peak flow, mean discharge, and flow variability were characterized by the potential of sediment detachment and delivery. In addition, T was significantly correlated with *FV* and SY. From the perspective of hydrology, flood duration determined the time length of channel erosion and sediment transport course, meanwhile, serves as an influencing factor of flow variability at the event scale. The total precipitation was statistically significant ($p < 0.01$) correlated to H, Q_p, and Q_m, thus the fluctuation of precipitation would led to corresponding hydrological response. No remarkable or weaker correlations were observed between the total precipitation and the suspended sediment concentration (SSC and S_{max}). However, the total rainfall was significant relative to SY, and the rainfall intensity had a significant impact on SSC and S_{max}.

3.3. Flood event classification

Fig. 3 exhibits four different patterns of the 112 flood events ($p < 0.01$). The scatters of discrimination functions for single flood pattern were well accumulated in four regions, indicating that the clustering result is relatively rational. The scatters of pattern C were relatively decentralized, whereas the scatters of Pattern B and Pattern D were more compacted. Furthermore, the boundary of Patterns B, C, and D was blurry, whereas Pattern A was relatively far from the other three patterns. The distribution of scatters suggested that the flood features of Patterns B, C, and D showed some similarity and Pattern A was obviously different from the others. Therefore, the two events included in Pattern A could be considered as extreme events.

Fig. 4 shows the characteristics of hydrological variables for

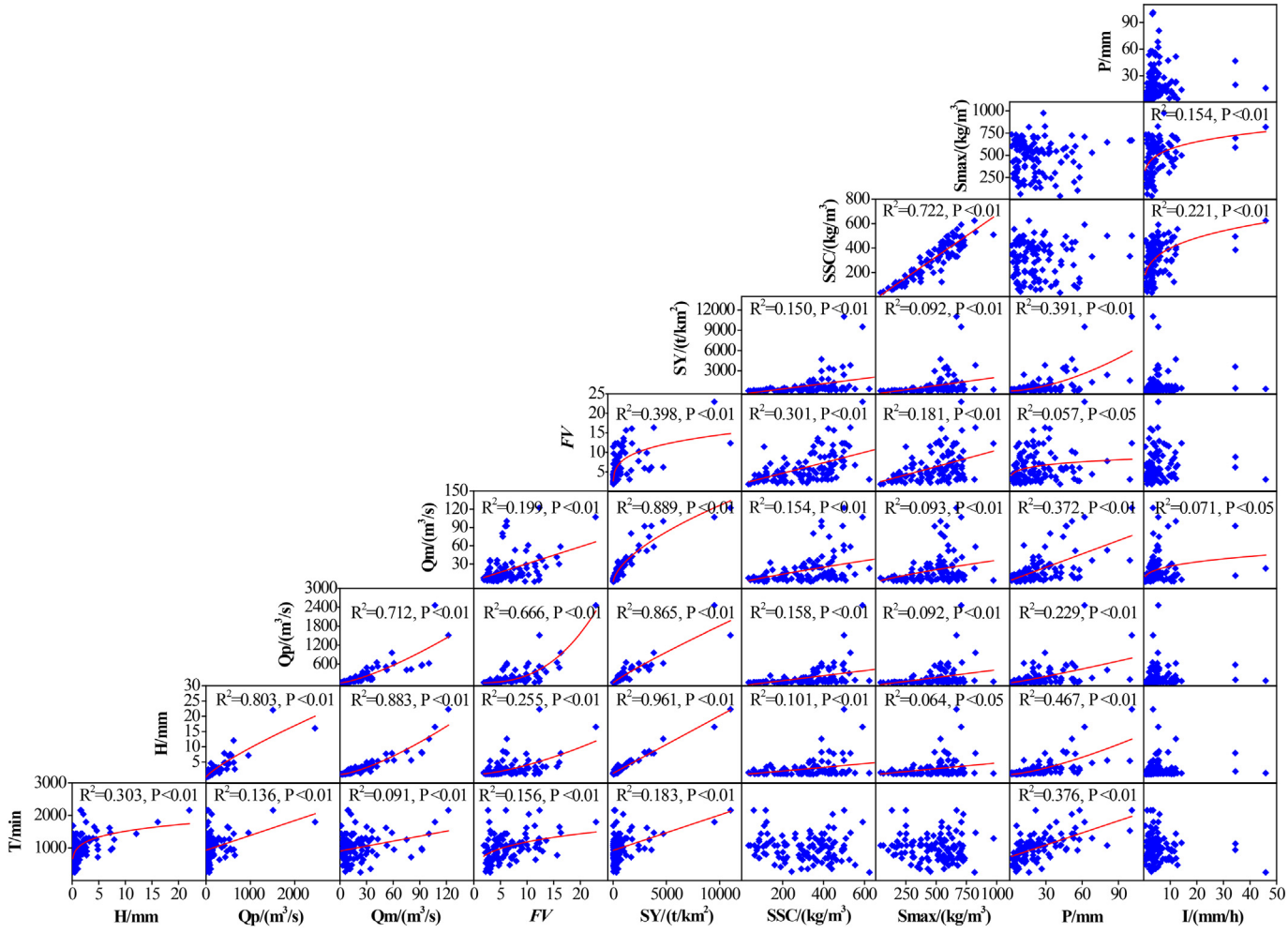

Fig. 2. Correlation analysis between runoff and sediment variables.

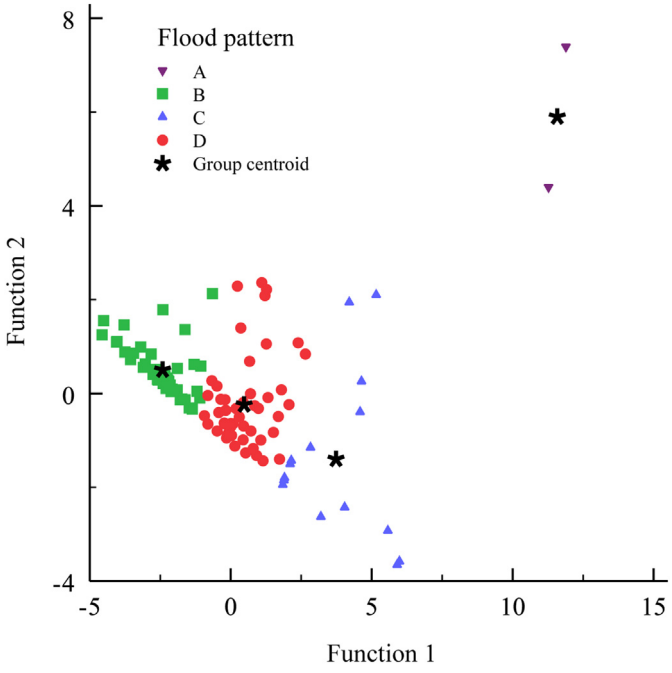

Fig. 3. Discriminant analysis on different flood patterns.

different flood patterns. Among all the flood events, only two events belonged to Pattern A, having longest flood duration, the highest runoff depth, the largest flood peak discharge and the maximum flood variability. A total of 43 flood events belonged to Pattern B. They were characterized by the shortest duration and flood variability, the lowest flood peak discharge and flow depth. Flood events of Pattern C (15 events) had long flood duration, high peak flow, large runoff depth, and high flood variability. Pattern D (52 events), which was characterized by a medium runoff depth, medium flow variability, medium duration, and medium peak flow, was the most commonly type of flood events. In contrast, the hydrological variables of Pattern C exhibited higher variability compared with those of Pattern B and Pattern D. For example, H ranged from 0.120 to 4.827 mm for Pattern B, but from 0.178 to 12.067 mm for Pattern C.

3.4. Flow-sediment relationship under various flood patterns

In general, sediment yield of flood events depend, to a great extent, on the combined effect of the runoff-related factors. Stepwise multiple regressions were conducted to determine the major controlling hydrological variables affecting event sediment yield across different flood patterns. Eqs. (8)–(10) showed the fundamental relationship formula between hydrological factors and event sediment yield. The events in Pattern A and Pattern C were merged into one pattern to perform regression analysis due to their similarities and the limited number of floods in Pattern A.

$$SY = e^{5.73}H^{1.17},\ R^2 = 0.972,\ p \le 0.01\,(Pattern\_A\ \&\ Pattern\_C) \quad (8)$$

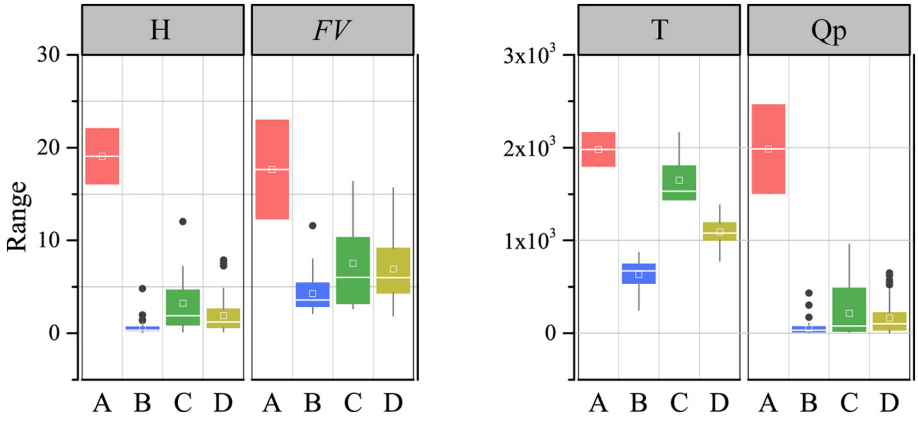

Fig. 4. Characteristics of flood events in different patterns.

$$SY = e^{8.98}H^{1.03}T^{-0.48},\ R^2 = 0.952,\ p \le 0.01\,(Pattern\_B) \quad (9)$$

$$SY = e^{9.69}H^{1.21}T^{-0.58},\ R^2 = 0.947,\ p \le 0.01\,(Pattern\_D) \quad (10)$$

According to Eqs. (8)–(10), the hydrological variables (H and T) influencing SY varied with different flood patterns. The event sediment yield of Pattern A and Pattern C (large flood events) were mainly positively determined by runoff depth. No statistically significant linkage between flood duration and event sediment yield was observed for the two flood patterns. In terms of Pattern B and Pattern D (medium and small flood events), the two runoff parameters were all included to estimate the sediment yield, and the event sediment yield had positive correlations with flow depth, whereas a negative correlation with flood durations.

3.5. Hysteretic loops

The SSC-Q hysteresis loops were further applied to investigate the dynamic changes of the relationship between suspended sediment concentration and runoff. Table 4 presents different types of hysteresis loops for different flood patterns in the Xichuan River catchment. Obviously, counter-clockwise and figure-eight loops were the dominant hysteresis loops types in all recorded flood events, which accounted for over 74% of the total events. Of the 112 events, forty-three events had a counter-clockwise loop, forty followed the eight-shaped clockwise loop and twenty seven were complex hysteresis, and only two events belonged to clockwise loop. With respect to the quantity of Pattern B, 21/43 flood events showed an anticlockwise hysteretic loop during the whole period, fifteen of the 43 flood events presented figure-eight hysteresis loops, and seven events had a clockwise hysteretic loop (Table 4). The complex hysteresis loops were the main type for Pattern C, including eight complex hysteresis loops, five counter-clockwise hysteresis loops and two figure-eight hysteresis loops. For the Pattern D, the figure-of-eight-shaped hysteretic loop was the main type, and only two clockwise hysteretic loops were found in this pattern. All the events in pattern A belonged to complex hysteresis loops. This indicated that complex hysteresis loops took up the highest proportion for the large flood events, whereas the counter-clockwise loops appeared more frequently in the relatively small events.

Table 4
Hysteresis loops analysis of different flood patterns.

Flood pattern	Hysteretic loops			
	Complex	Counter-clockwise	Figure-eight	Clockwise
A	2	0	0	0
B	7	21	15	0
C	8	5	2	0
D	10	17	23	2
Total	27	43	40	2

Various patterns of hysteretic loops have been found in the catchment. Complex hysteresis loops included events with two or more types loop frequently (i.e. different hysteresis loops coexisted in the same flood through different combinations and order). Fig. 5 shows four examples of complex hysteresis loops of different flood patterns. Generally, the complex hysteresis loops had several runoff peak values and sediment peaks. For instance, the event that recorded on July 5, 1977 (Fig. 5a) lasted up to approximately 36 h, and consisted of three flood peak discharge values and four sediment peaks. Furthermore, the fluctuation of flow discharge and suspended sediment concentration was quite large. Therefore, the corresponding hysteresis loops (Fig. 5b) presented extremely complex situation. As shown in Fig. 5b and d, the hysteresis loop presented complex mixtures of clockwise and anticlockwise loops.

When the flow discharge reached the peak prior to the suspended sediment concentration during one flood event, the counter-clockwise hysteretic loop could be identified. Two typical counter-clockwise loops characterized the floods of July 6, 1986 and June 27, 1988. As shown in Fig. 6, a sharp increase in sediment concentration was detected as runoff discharge increased, and the flow discharge peaked firstly. The SSC was significantly lower in the rising stage of the hysteresis loops graph than in the falling stage with flow discharge level being equal. For instance, when the discharge value was in a level of 53.6 $m^3 \cdot s^{-1}$ during the event of June 27, 1988 (Fig. 6d), the SSC of rising stage was 236 $kg \cdot m^{-3}$, while the value was up to 642 $kg \cdot m^{-3}$ on the recession stage. In addition, the changing tendency of runoff and sediment concentration as well as hysteresis were basically coincident between the two flood patterns. The SSC peaked within hours following the runoff peak that was induced by rainstorm events, which further corroborated the site of sediment sources were remote from the gauging station.

As shown in Fig. 7, figure-eight hysteresis loops consisted of clockwise and anticlockwise loop. This type could be interpreted with two parts distinguishing by one point that SSC to Q ratio of the rising limb are equal to the ratio in the falling limb. Accordingly, the SSC/Q ratio in the rising stage were much less than that in the falling stage for low discharge, whereas the corresponding ratio presented the opposite situation for higher discharges (Fig. 7b and d).

Clockwise hysteretic loops were observed in the Xichuan River for the floods of July 26, 2013, July 5, 1988 (Fig. 8). When runoff peak lagged behind the SSC peak or the two variables peaked at the same time, a clockwise hysteresis occurred. Unlike the counter-clockwise hysteretic loops, the SSC was higher during the rising limb than the falling limb for a clockwise hysteretic loop. As shown in the hydrographs and sedigraphs (Fig. 8a and c), the SSC was in a trend of sharp increase at the initial stage of the flood event.

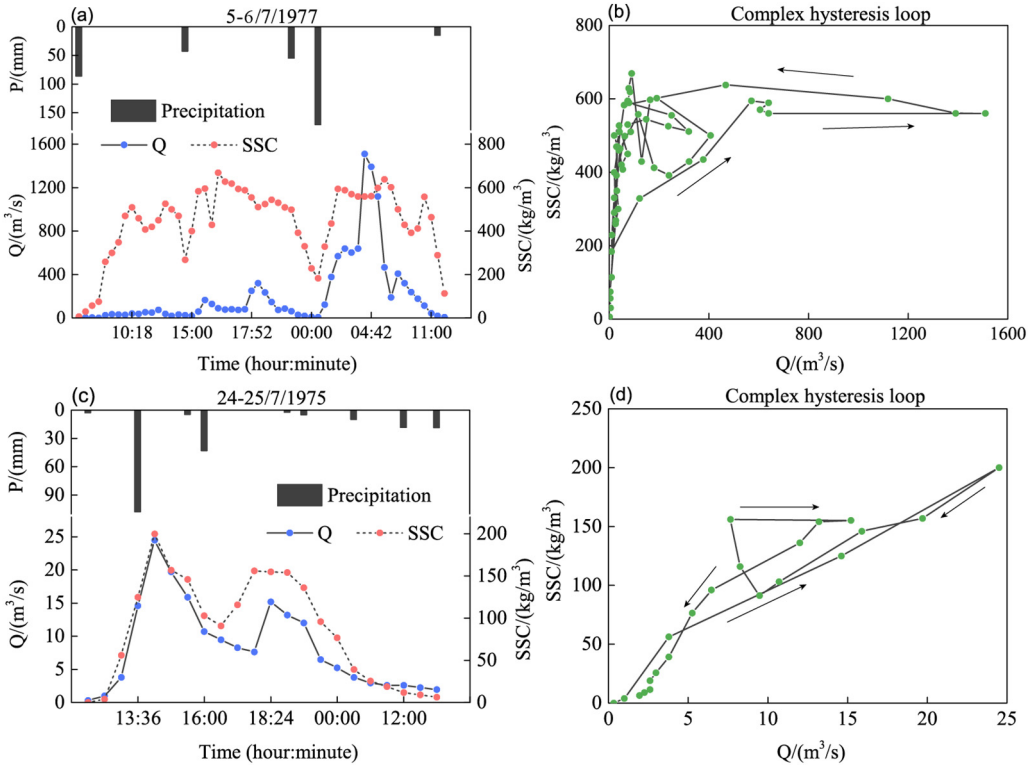

Fig. 5. Complex hysteresis loops.

4. Discussion

4.1. Hydrologic and sediment characteristics

Surface runoff was the dominant driving force for sediment transport. Generally, the runoff depth could be applied to reflect the sediment transport capacity of surface runoff, which had been verified in many studies (Zhang et al., 2016; Zheng et al., 2008; Zheng et al., 2013). Their results indicated that rainfall alone did not control sediment transport in such highly dynamic systems but worked in combination with the production, erosion and availability of sediment (whether stored in channels or confined in badlands). The correlation

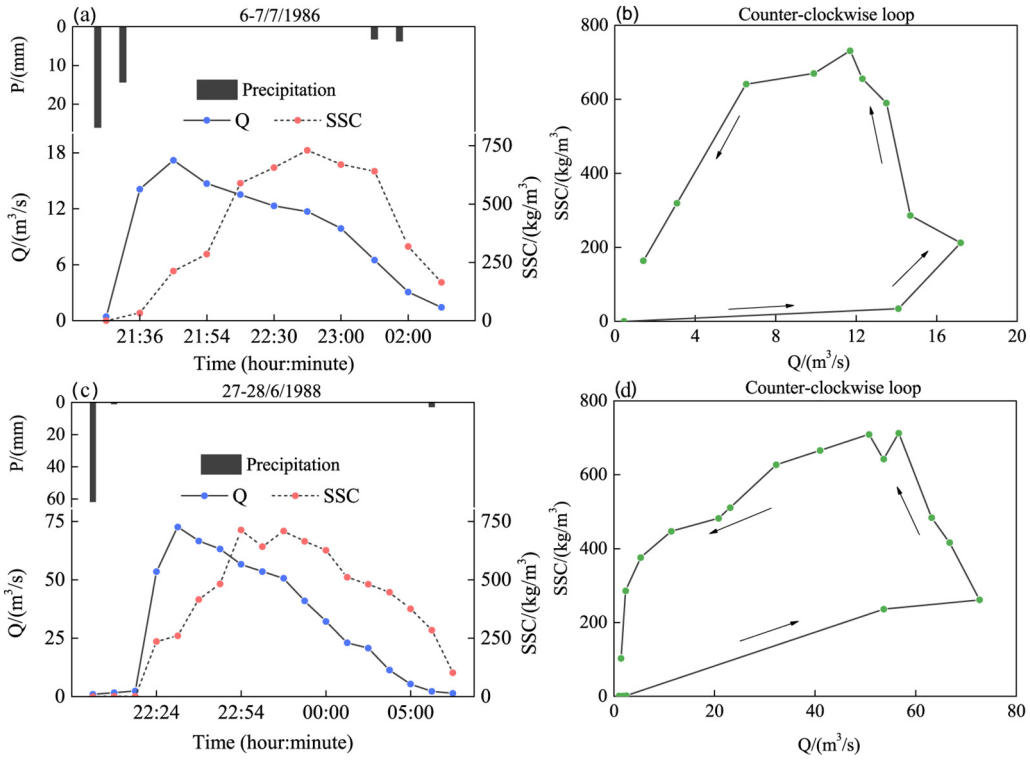

Fig. 6. Counter-clockwise hysteretic loops.

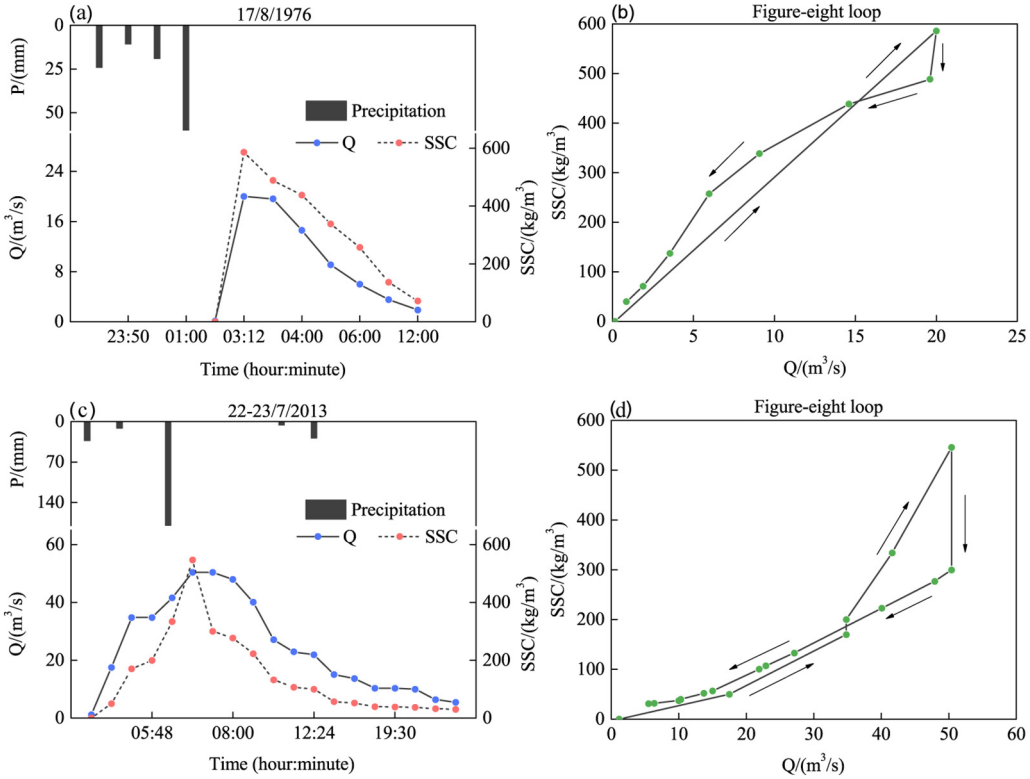

Fig. 7. Figure-eight hysteretic loops.

analysis in the present study suggested that the main hydrologic variables (H, Q_p, and Q_m) displayed a significant correlation with SY in the study period (Fig. 2). This finding confirmed that runoff discharge was the most relevant factor controlling the sediment yield in the study area (Zheng et al., 2008). Nevertheless, relatively low correlation was observed between the SSC and the hydrological variables. The poor SSC-Q statistical relationship was consistent with other researches of event-related suspended sediment dynamics (Estrany et al., 2009; Pierson,

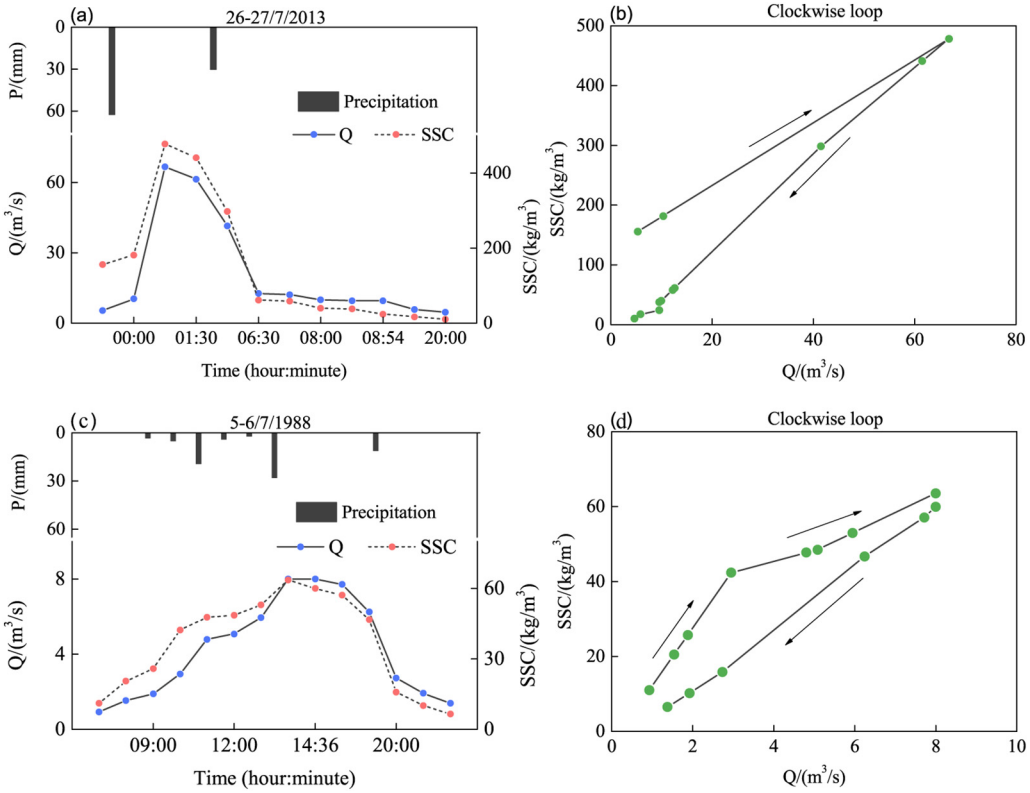

Fig. 8. Clockwise hysteretic loops.

2005). Zheng et al. (2012) pointed out that SSC had no correlation with H at various spatial scales from the hilltop to the watershed for a single event. One possible reason for this is that sediment supply of Loess Plateau was generally abundant without limit and thus SSC depended largely on the transport capacity of flows instead of runoff volume (i.e. small-scale floods could generate hyper-concentrated flow, rather, the SSC might also be low level for large floods). A similar relatively weak relationship had been detected between S_{max} and Q_{max} (Fig. 2), and further verified previously studied results that sediment response did not depend solely on discharge values (Lenzi and Marchi, 2000; Walling and Webb, 1982).

The spatial-temporal heterogeneity of precipitation played an indispensable role in sediment yield which was induced by soil erosion. In this study, rainfall intensity had a weak or non-significant relationship with runoff variables and SY, while a dramatic correlation with SSC. This might be due to the fact that the high intensity storm had a destructive effect on the soil surface and was prone to produce hyper-concentrated flow. And previous research in the loess regions has also shown that high sediment concentrations could be observed even when flow discharge was quite low due to the high intensity rainstorms (Xu, 2004). These analysis above illustrated that SY was mainly dependent upon the magnitude of flood runoff volumes (depth), whereas event-based SSC and S_{max} were mainly influenced by the rainfall intensity.

4.2. Influence of flood patterns on sediment yield

Previous studies used correlation analyses to investigate the relationships between the runoff and event sediment yield (Cai et al., 2004; Lane et al., 1997). For the highly erodible catchment of the Loess Plateau, the SY-H relationship could be well modeled using the proportional model proposed by Zheng et al. (2007) and Zheng et al. (2008). This model was valid for various scales from the hill slope to the large-sized catchment where easily erodible materials supply was sufficiently. As a result of some large-scale reforestation project, especially the "Grain for Green" Project, vegetation coverage and land use types in the Xichuan River catchment had significantly changed since 1990s (Fig. 9). Table 5 compares the land use areas at the two dates (1990 and 2010). A remarkable increase in grassland and an evident decrease in arable land could be identified. In 1990, grassland covered approximately 37.18% of the entire catchment, whereas in 2010, grassland coverage was 46.87%, corresponding to a remarkable coverage increase in the catchment. In contrast, the area of arable land decreased from 301.09 km^2 in 1990 to 218.22 km^2 in 2010. As with land use impacts considered above, the runoff and sediment response of the catchment is likely to have changed greatly. Numerous studies have confirmed that human-induced ecological restoration played an important role in the reduction of runoff and subsequent sediment load on the Loess Plateau (Rustomji et al., 2008; Zhao et al., 2016). However, there might be

Table 5
Land use changes as of two dates in the Xichuan River catchment.

Area	1990		2010	
	km^2	%	km^2	%
Grass land	297.82	37.18	375.44	46.87
Forests	198.95	24.84	203.68	25.43
Arable land	301.09	37.59	218.22	27.25
Water body	2.59	0.32	0.19	0.02
Urban area	0.45	0.06	3.47	0.43
Bare/unused land	0.10	0.01	0.00	0.00

differences in the mechanism of sediment reduction among different flood patterns. As Zheng et al. (2008) and Zheng et al. (2013) addressed, the runoff-sediment relationship remains relatively invariant for large runoff events, and this relationship do not change with the implement of human-dominated vegetation practices for soil conservation. Consequently, the reduction of sediment export at the outlet could be attributed to the decrease the flood runoff amount for large flood events (i.e. the sediment-reduction efficiency is approximately equal to the runoff-reduction efficiency). This may lead to the failure of the vegetation and other slope land measures in controlling sediment yield at the catchment scale. Nevertheless, for the relatively minor flood events, the runoff-sediment relationship might be unsteady. As ecological restoration measures continue, the runoff-sediment relationships of small and medium runoff events will inevitably change. Therefore, determining the mechanism of sediment reduction will be beneficial to assess soil erosion control strategies effectively. The contribution of different flood patterns to the summed sediment load was 24.5% (1.48×10^7 t), 11.2% (6.77×10^6 t), 21.4% (1.29×10^7 t) and 42.9% (2.59×10^7 t) for Patterns A, B, C, and D, respectively. For the sediment load of single event, the contribution rate of only two flood events (Pattern A) reached up to 24.5%. This was consistent with other previous studies in that sediment load of the watershed primarily came from a small number of flood events at the event scale (Estrany et al., 2009; Fang et al., 2012; Lana-Renault and Regüés, 2009). Furthermore, Table 6 shows that Pattern A produced the most SY, whereas Pattern B produced the least SY, and the SY produced by Pattern A was significantly larger than that by Patterns B, C, and D. In general, most relatively minor flood contributed extremely limited sediment to overall sediment yield at the basin outlet due to low SY though the frequency was high. In this study, Pattern B had the extremely frequent flood events. However, it produced the lowest total sediment load in the all patterns. Nevertheless, the crucial role that these small flood events in geomorphological processes of gully and channel could not be neglected (Zheng et al., 2008). Especially for the Loess Plateau, where the sand content was comparatively high, a mass of coarse sediment

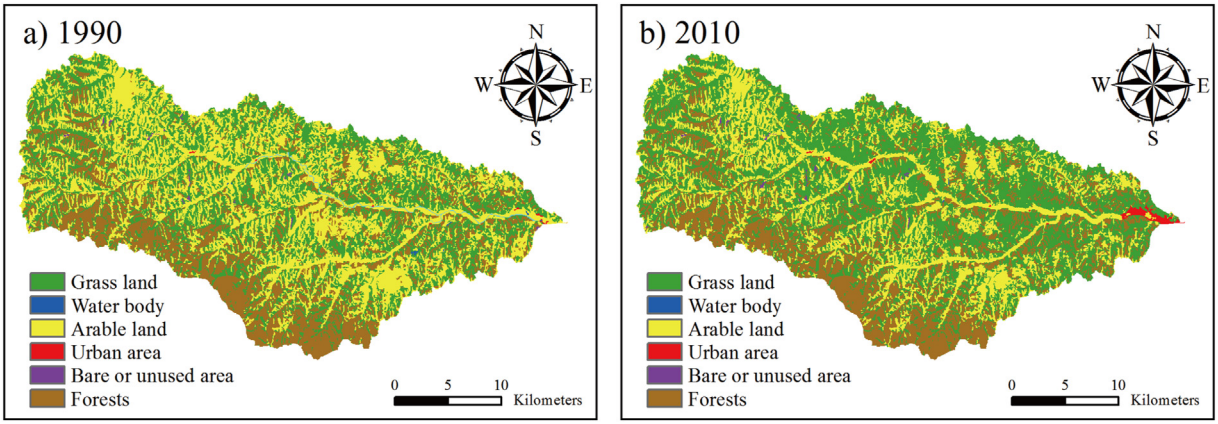

Fig. 9. Land use changes in the Xichuan River catchment.

Table 6
Main statistical variables of sediment for different flood patterns.

Flood pattern	Main sediment variable		
	SY ($t \cdot km^{-2}$)	SSC ($kg \cdot m^{-3}$)	S_{max} ($kg \cdot m^{-3}$)
A	10,275.33	545.95	688.50
B	218.84	321.41	503.35
C	1196.39	280.42	485.07
D	693.84	309.32	453.11

derived from splash erosion and scoured erosion might deposit in channel temporarily on account of low-magnitude flow transport capacity. The stored sediment would serve as the primary source during the subsequent large-magnitude events. Therefore, the sediment control should firstly aimed at large sediment-producing patterns such as Pattern A and Pattern C. However, the contribution of small-sediment-producing events to sediment delivery should never be ignored.

4.3. Sediment dynamics

The event-based sediment dynamics can be investigated through the analysis of the SSC-Q hysteretic loops. In this study, the majority of flood events occurring during the study period presented counter-clockwise hysteretic loops. However, in contrast to our study, clockwise loops are more common (usually were observed in small catchments with humid climate) in most previous literature (Brasington and Richards, 2000; Heidel, 1956; Jansson, 2002; Lenzi and Marchi, 2000; Rovira and Batalla, 2006; Williams, 1989). This phenomenon could be attributed to the condition of non-limited sediment supply environment of the catchment, the intensive sediment carrying capability of hyperconcentrated flow, and the spatial distribution of eroded rainstorm. Unlike many catchments around the world, which belonged to 'supply-limited' sediment delivery system, sediment supply of the Loess Plateau is generally abundant without limit and prone to produce the hyperconcentrated flow. In general, soil erosion induced by erosive rainfall could be considered as a detachment process during the rising limb, serving as the sediment source, whereas transport process may dominate the receding stage. For the counter-clockwise hysteretic loops, the large amount of erodible materials were from erosion areas on slope zones (Fig. 10), located mainly in the upper part of the catchment. Therefore, sediment was transported to the river from remote areas after the runoff peak, resulting in the inconsistence between the runoff peak and sediment peak. In addition, flow discharge presented a decreasing tendency with rainfall dropping during the recessing stage, whereas sediment concentration remained high. The inconsistency of Q and SSC resulted in higher sediment concentrations during the recessing stage than during the rising stage for a given flow discharge.

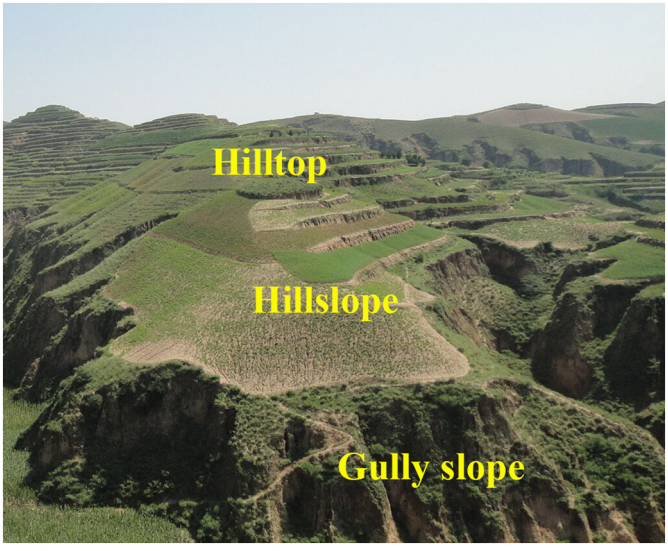

Fig. 10. Typical slope–gully system in the hilly region of the Chinese Loess Plateau.

Counter-clockwise hysteretic loops seems most likely to be explained by the distance between sediments-producing area and the outlet (Lenzi and Marchi, 2000). Similarly, the spatial heterogeneity of rainfall across the catchment also produce various sediment sources, which might have certain influence on the distance between sediment sources and gauging stations (Cashman and Potter, 2006; Mano et al., 2009; Zhao et al., 2017). Similar results have been reported by other researchers (Fang et al., 2008; Tian et al., 2016), suggesting that the counter-clockwise hysteretic loop predominated the other catchments on the Loess Plateau. An investigation by Zhao et al. (2017) implied that the reason why the complex and anti-clockwise hysteresis dominated the Huangfuchuan and Yanhe catchments was the high variability of the rainfall for the large-scale basin.

According to Williams (1989), hysteresis loops are influenced by various factors, including the runoff amount, rainfall intensity, rainfall duration, rainfall distribution and floodwater travel distances. Lana-Renault and Regüés (2009) suggested that the counter-clockwise hysteresis events were characterized by limited discharge, reduced sediment yield and high SSC. In addition, different hysteresis loops will have distinctive patterns in the hydrological and sedimentary response. In the present study, flood duration associated with counter-clockwise loops were the shortest, and the total precipitation were generally low. By contrast, clockwise loops possessed the characteristic of the longest duration. The total rainfall amount associated with such events was moderate. The hydrological response and sediment response of such type was at the lowest level. There was few previous literature on the researches of figure-eight loop (Nadal-Romero et al., 2008; Williams, 1989). Buendia et al. (2016) pointed out that the figure-eight patterns had the characteristics of long duration at the event scale, and can be induced by various mechanisms. In that study, this type of hysteretic effect showed medium mean duration though including the longest-duration event, appearing primarily in Pattern B and Pattern D flood events for our research.

The SSC-Q hysteresis patterns were applied to deduce the distance of sediment availability widely in many studies published. Corresponding to different hysteresis types, the sediment yield in the watershed did not merely depend on the sediment of channel network driven by flow but also controlled by sediment production in headwater areas and the area close to outlet. Counter-clockwise, the peak of Q reached the outlet much prior to SSC peak or synchronously, whose sediment source theoretically located in headwater areas. Buendia et al. (2016) reported in the River Isábena that the sediment availability of counter-clockwise loops were widely distributed throughout the catchment and would not be depleted rapidly. A number of studies suggested that the clockwise loops were caused by depleting or flushing out sediment deposited near the catchment outlet (Rovira and Batalla, 2006; Smith and Dragovich, 2009). Additionally, Klein (1984) suggested that the clockwise hysteresis will present in circumstance when the sediment source was the channel itself or an adjacent area located close to the basin outlet. The flow velocity of hillslope was far slower than that of the channel. Therefore, supposing that the sediment came primarily from bank and channel erosion (the sediment deposited in the river bed and channel prior to flood event), the SSC and runoff would peak simultaneously, or the SSC peak preceded runoff peak, and thereby the clockwise loops occurred. During figure-eight events, the sediment supply were relatively complicated (Gentile et al., 2010). Part of the explanation might lie in the situation that the sediment accumulated close to the outlet were washed out at the initial phase, hence the SSC increased simultaneously with the runoff discharge. As the further exhaustion of limited sediment and decreasing in sediment availability, the SSC dropped sharply. Finally, the overland flow

receded gradually as the rainfall intensity decreased, while the sediment production decreased more slowly than runoff generation due to the recharge of sediment from upper area. Above all, based on the types of hysteresis loops, sediment availability as well as sediment sources could be generally determined.

5. Conclusion

A total of 112 events occurred during 1974–1989 and 2007–2013 were selected to assess the runoff-sediment relationship and the suspended sediment dynamics in the Xichuan River catchment from the Loess Plateau. All the flood events were classified into four patterns with flood duration, runoff depths, peak flow and flow variability. Patterns A and C were characterized by its low frequency and extremely high sediment yield amount at a single event scale. Therefore, further attention must be paid to the two flood patterns to control sediment yield of the catchment.

Correlation analysis showed that runoff depth was the key variable influencing event sediment yield. The hydrological variables that affected the sediment yield varied across different flood patterns. Event sediment yield of Patterns A and C were positively correlated with runoff depth and flood peak discharge. For Pattern B, SY has strong positive correlations with flow depth and flood peak discharge, and negative correlations with flood duration. As for Pattern D, positive and negative relationships were detected between SY and runoff depth as well as between SY and flood duration, respectively.

SSC-Q hysteretic loops were applied to reflect the dynamics of suspended sediment and deduce the sediment source approximately. The majority of flood events presented counter-clockwise hysteretic loops across the entire study period, resulting from the non-limited sediment supply environment and the spatial heterogeneity of rainfall. The dominant shape of the hysteresis reflected that the sediment source of the Xichuan River catchment was mainly located in headwater areas.

Acknowledgments

The work was financially supported by the National Key Scientific Research Project (Grant No. 2016YFC0402401), the National Natural Science Foundation of China (Grant Nos. 41671285, 41671279), and Special Funds for Scientific Research Programs of the State Key Laboratory of Soil Erosion and Dryland Farming on the Loess Plateau (Grant No. A314021403-Q2).

References

Asselman, N.E.M., 1999. Suspended sediment dynamics in a large drainage basin: the River Rhine. Hydrol. Process. 13, 1437–1450.
Bača, P., 2008. Hysteresis effect in suspended sediment concentration in the Rybárik basin, Slovakia (Effet d'hystérèse dans la concentration des sédiments en suspension dans le bassin versant de Rybárik (Slovaquie)). Hydrol. Sci. J. 53, 224–235.
Bai, Y.M., 2011. Effect of returning farmland to forests to benifit of soil and water conservation in Xichuanhe River Basin. J. Water Resour. Water Eng. 22, 176–178 (in Chinese).
Brasington, J., Richards, K., 2000. Turbidity and suspended sediment dynamics in small catchments in the Nepal Middle Hills. Hydrol. Process. 14, 2559–2574.
Buendia, C., Vericat, D., Batalla, R.J., Gibbins, C.N., 2016. Temporal dynamics of sediment transport and transient in-channel storage in a highly erodible catchment. Land Degrad. Dev. (4), 1045–1063.
Cai, Q.G., Liu, J.G., Liu, Q.J., 2004. Research of sediment yield statistical model for single rainstorm in Chabagou drainage basin. Geogr. Res. 23, 433–439 (in Chinese).
Cashman, E., Potter, K., 2006. Modelling the impacts of climate variability on sediment transport. IAHS Publ. 306, 611–619.
Deasy, C., Brazier, R., Heathwaite, A., Hodgkinson, R., 2009. Pathways of runoff and sediment transfer in small agricultural catchments. Hydrol. Process. 23, 1349–1358.
Eder, A., Strauss, P., Krueger, T., Quinton, J.N., 2010. Comparative calculation of suspended sediment loads with respect to hysteresis effects (in the Petzenkirchen catchment, Austria). J. Hydrol. 389, 168–176.
Estrany, J., Garcia, C., Batalla, R.J., 2009. Suspended sediment transport in a small Mediterranean agricultural catchment. Earth Surf. Process. Landf. 34, 929–940.
Fang, H.Y., Cai, Q.G., Chen, H., Li, Q.Y., 2008. Temporal changes in suspended sediment transport in a gullied loess basin: the lower Chabagou Creek on the Loess Plateau in China. Earth Surf. Process. Landf. 33, 1977–1992.
Fang, H.Y., Li, Q.Y., Cai, Q.G., Liao, Y.S., 2011. Spatial scale dependence of sediment dynamics in a gullied rolling loess region on the Loess Plateau in China. Environ. Earth Sci. 64, 693–705.
Fang, N.F., Shi, Z.H., Li, L., Guo, Z.L., Liu, Q.J., Ai, L., 2012. The effects of rainfall regimes and land use changes on runoff and soil loss in a small mountainous watershed. Catena 99, 1–8.
Gentile, F., Bisantino, T., Corbino, R., Milillo, F., Romano, G., Liuzzi, G.T., 2010. Monitoring and analysis of suspended sediment transport dynamics in the Carapelle torrent (Southern Italy). Catena 80, 1–8.
Heidel, S.G., 1956. The progressive lag of sediment concentration with flood waves. EOS Trans. Am. Geophys. Union 37, 56–66.
Jansson, M.B., 2002. Determining sediment source areas in a tropical river basin, Costa Rica. Catena 47, 63–84.
Klein, M., 1984. Anti clockwise hysteresis in suspended sediment concentration during individual storms: Holbeck Catchment; Yorkshire, England. Catena 11, 251–257.
Lana-Renault, N., Regüés, D., 2009. Seasonal patterns of suspended sediment transport in an abandoned farmland catchment in the Central Spanish Pyrenees. Earth Surf. Process. Landf. 34, 1291–1301.
Lane, L.J., Hernandez, M., Nichols, M., 1997. Processes controlling sediment yield from watersheds as functions of spatial scale. Environ. Model. Softw. 12, 355–369.
Lefrançois, J., Grimaldi, C., Gascuel-Odoux, C., Gilliet, N., 2007. Suspended sediment and discharge relationships to identify bank degradation as a main sediment source on small agricultural catchments. Hydrol. Process. 21, 2923–2933.
Lenzi, M.A., Marchi, L., 2000. Suspended sediment load during floods in a small stream of the Dolomites (northeastern Italy). Catena 39, 267–282.
López-Tarazón, J.A., Batalla, R.J., Vericat, D., Francke, T., 2009. Suspended sediment transport in a highly erodible catchment: the River Isábena (Southern Pyrenees). Geomorphology 109, 210–221.
Luk, S.H., 1997. Gully erosion and sediment transport in a small subtropical catchment, South China. Catena 29, 161–176.
Mano, V., Nemery, J., Belleudy, P., Poirel, A., 2009. Assessment of suspended sediment transport in four alpine watersheds (France): influence of the climatic regime. Hydrol. Process. 23, 777–792.
Mu, X.M., Zhang, L., McVicar, T.R., Chille, B., Gao, P., 2007. Analysis of the impact of conservation measures on stream flow regime in catchments of the Loess Plateau, China. Hydrol. Process. 21, 2124–2134.
Nadal-Romero, E., Regüés, D., Latron, J., 2008. Relationships among rainfall, runoff, and suspended sediment in a small catchment with badlands. Catena 74, 127–136.
Oeurng, C., Sauvage, S., Sánchez-Pérez, J.M., 2010. Dynamics of suspended sediment transport and yield in a large agricultural catchment, southwest France. Earth Surf. Process. Landf. 35, 1289–1301.
Peng, T., Wang, S.J., 2012. Effects of land use, land cover and rainfall regimes on the surface runoff and soil loss on karst slopes in southwest China. Catena 90, 53–62.
Pierson, T.C., 2005. Hyperconcentrated flow—transitional process between water flow and debris flow. In: Debris-flow Hazards and Related Phenomena. Springer, pp. 159–202.
Porto, P., Walling, D.E., Callegari, G., 2011. Using 137Cs measurements to establish catchment sediment budgets and explore scale effects. Hydrol. Process. 25, 886–900.
Rovira, A., Batalla, R.J., 2006. Temporal distribution of suspended sediment transport in a Mediterranean basin: the Lower Tordera (NE SPAIN). Geomorphology 79, 58–71.
Rustomji, P., Zhang, X.P., Hairsine, P.B., Zhang, L., Zhao, J., 2008. River sediment load and concentration responses to changes in hydrology and catchment management in the Loess Plateau region of China. Water Resour. Res. 44 (7), W00A04.
Sayer, A.M., Walsh, R.P., Bidin, K., 2006. Pipeflow suspended sediment dynamics and their contribution to stream sediment budgets in small rainforest catchments, Sabah, Malaysia. For. Ecol. Manag. 224, 119–130.
Smith, H.G., Dragovich, D., 2009. Interpreting sediment delivery processes using suspended sediment-discharge hysteresis patterns from nested upland catchments, south-eastern Australia. Hydrol. Process. 23, 2415–2426.
Soler, M., Latron, J., Gallart, F., 2008. Relationships between suspended sediment concentrations and discharge in two small research basins in a mountainous Mediterranean area (Vallcebre, Eastern Pyrenees). Geomorphology 98, 143–152.
Sun, L.Y., Yan, M., Cai, Q.G., Fang, H.Y., 2016. Suspended sediment dynamics at different time scales in the Loushui River, south-central China. Catena 136, 152–161.
Tang, K., Zhang, P., Wang, B., 1991. Soil erosion and eco-environment changes in Quaternary. Quat. Res. 4, 49–56.
Tian, P., Zhai, J.Q., Zhao, G.J., Mu, X.M., 2016. Dynamics of runoff and suspended sediment transport in a highly erodible catchment on the Chinese Loess Plateau. Land Degrad. Dev. 27, 839–850.
Walling, D.E., Webb, B., 1982. Sediment availability and the prediction of storm-period sediment yields. Recent Dev. Explanation Prediction Erosion Sediment Yield 137, 327–337.
Wang, H.J., Yang, Z.S., Saito, Y., Liu, J.P., Sun, X.X., Wang, Y., 2007. Stepwise decreases of the Huanghe (Yellow River) sediment load (1950–2005): impacts of climate change and human activities. Glob. Planet. Chang. 57, 331–354.
Wang, F., Hessel, R., Mu, X.M., Maroulis, J., Zhao, G.J., Geissen, V., Ritsema, C., 2015. Distinguishing the impacts of human activities and climate variability on runoff and sediment load change based on paired periods with similar weather conditions: a case in the Yan River, China. J. Hydrol. 527, 884–893.
Williams, G.P., 1989. Sediment concentration versus water discharge during single hydrologic events in rivers. J. Hydrol. 111, 89–106.
Xu, J.X., 2004. Hyperconcentrated flows in the slope-channel systems in gullied hilly areas on the loess plateau, China. Geogr. Ann. Ser. B Phys. Geogr. 86A, 349–366.
Yellow River Conservancy Committee, 1974–1989, 2007–2013. Hydrological Year Book of the Yellow River. Yellow River Conservancy Press.
Zabaleta, A., Martinez, M., Uriarte, J.A., Antiguedad, I., 2007. Factors controlling

suspended sediment yield during runoff events in small headwater catchments of the Basque Country. Catena 71, 179–190.
Zhang, L.T., Li, Z.B., Wang, S.S., 2016. Spatial scale effect on sediment dynamics in basin-wide floods within a typical agro-watershed: a case study in the hilly loess region of the Chinese Loess Plateau. Sci. Total Environ. 572, 476–486.
Zhao, G.J., Mu, X.M., Wen, Z.M., Wang, F., Gao, P., 2013. Soil erosion, conservation, and eco-environment changes in the loess plateau of China. Land Degrad. Dev. 24, 499–510.
Zhao, G.J., Mu, X.M., Jiao, J.Y., An, Z.F., Klik, A., Wang, F., Jiao, F., Yue, X.L., Gao, P., Sun, W.Y., 2016. Evidence and causes of spatiotemporal changes in runoff and sediment yield on the Chinese Loess Plateau. Land Degrad. Dev. 28, 579–590.
Zhao, G.J., Yue, X.L., Tian, P., Mu, X.M., Xu, W.L., Wang, F., Gao, P., Sun, W.Y., 2017. Comparison of the suspended sediment dynamics in two Loess Plateau catchments, China. Land Degrad. Dev. 28, 1398–1411.
Zheng, M.G., Cai, Q.G., Cheng, Q.J., 2007. Sediment yield modeling for single storm events based on heavy-discharge stage characterized by stable sediment concentration. Int. J. Sediment Res. 22, 208–217.
Zheng, M.G., Cai, Q.G., Cheng, Q.J., 2008. Modelling the runoff-sediment yield relationship using a proportional function in hilly areas of the Loess Plateau, North China. Geomorphology 93, 288–301.
Zheng, M.G., Yang, J.S., Qi, D.L., Sun, L.Y., Cai, Q.G., 2012. Flow–sediment relationship as functions of spatial and temporal scales in hilly areas of the Chinese Loess Plateau. Catena 98, 29–40.
Zheng, M.G., Qin, F., Yang, J.S., Cai, Q.G., 2013. The spatio-temporal invariability of sediment concentration and the flow–sediment relationship for hilly areas of the Chinese Loess Plateau. Catena 109, 164–176.
Zheng, M.G., Li, R.K., He, J.J., 2015. Sediment concentrations in run-off varying with spatial scale in an agricultural subwatershed of the Chinese Loess Plateau. Hydrol. Process. 29, 5414–5423.